16TH EUROPEAN CONFERENCE ON EARTHQUAKE ENGINEERING THESSALONIKI 18 - 21 JUNE 2018

MODELING AND SEISMIC RESPONSE ANALYSIS OF THE FULLY JOINTLESS SEMI-INTEGRAL BRIDGE

Yongchun MA[1], Xudong SHAO[2], Jingjing WANG[3], Guobin, BU[4]

ABSTRACT

Jointless bridge has been proven to be of excellent seismic performance. In this study, seismic performance of an innovative jointless bridge, namely fully jointless semi-integral bridge (FJSIB), is analyzed. The FJSIB not only eliminates all the joints in the bridge but also replace the two joints between bridge and road with an approach pavement system which is used to accommodate the expansion and shrinkage deformation from the bridge deck. The interfacial friction between reinforced concrete approach pavement (RCAP) and subgrade as well as the soil-structure interaction between ground beam and embankment are beneficial to reduce the seismic response of the bridge. The modeling of the approach pavement system (APS) is complex. RCAP is an axial-bending-shear component modeled by the force-based beam-column element with uniaxial section involved. Earth pressure models of rigid retaining wall are suitable for the soil-anchored ground beam interaction and modeled with the extended hyperbolic force-displacement formulation model (EHFD). The 3D nonlinear finite element model of FJSBs is established by the OpenSees software and the seismic response analysis is carried out by the nonlinear time-history analysis. The results show that the seismic response of the FJSB are only 1/(1.8～2.3) that of the continuous girder bridges, which proves excellent seismic performance of the FJSB. The FJSBs can be used in new bridge construction as well as old bridge retrofitting, especially in the strong earthquake area.

Keywords: Jointless bridge; Seismic response; Semi-integral; Approach pavement system; OpenSees

1. INTRODUCTION

While integral and semi-integral abutment brieges (IABs, SIABs, namely conventional jointless bridges) have no joint in the superstructure, two road-bridge expansion joints are still kept at the approach slab end to accommodate the expansion and shrinkage deformation from the bridge deck (Maruri and Petro 2005). In order to completely achieve “zero maintenance” of the small and medium beam bridges, an innovative fully jointless semi-integral bridge (FJSIB) which replace the road-bridge expansion joint with an approach pavement system (APS) has been proposed in China (Jing and Shao 2009) (the research team of the author). The approach pavement system includes two crucial elements: one is a reinforced concrete approach pavement (RCAP) in which evenly distributed cracks are preseted and can effectively accommodate the expansion and shrinkage deformation like a spring; the other is a ground beam which is embedded in the embankment to anchor the end of RCAP.

Many earthquake events and seismic studies have proven that the conventional jointless bridges have excellent seismic performance owing to the good integrity and soil-structure interaction (Hoppe and Gomez 1996). Similarly, the ground beam, RCAP and continuous girder (deck) of the fully jointless semi-integral bridge are integrated together; the soil-ground beam interaction, the interfacial friction between RCAP and subgrade and the hysteretic behaviour of RCAP can dissipate sufficient seismic energy. These characteristics of FJSIB mentioned above are beneficial for earthquake resistance.

[1] Assistant Professor, Hunan University of Technology, Zhuzhou, China, 191098470@qq.com
[2] Professor, Hunan University, Changsha, China, shaoxd@163.com
[3]Assistant Professor, Hunan University of Technology, Zhuzhou, China, wangjj@hut.edu.cn
[4]Assistant Professor, Hunan University of Technology, Zhuzhou, China, buguobin@hut.edu.cn

Up to now, the author has simplified the approach pavement system as a linear elastic boundary and the qualitative results of the modal analysis and response spectrum analysis show that the APS can significantly reduce the dynamic response of the superstructure (Ma et al. 2013). However, for seismic design or seismic assessment, it needs to carry out the accurate quantitative analysis with the nonlinearity of APS considered. Reviewing the literature, it is found that the dynamic time-history analysis based on simplified nonlinear finite element model of jointless bridge is the most efficient and precise method (Wilson 1988, Faraji 2001, Ní Choine et al. 2015). Therefore in this paper, a prestressed concrete continuous box girder bridge in Kun-ming is used as the "reference" case. The approach pavement system is crucial and its detailed modeling method will be given; The FEM of the continuous girder bridge and the fully jointless semi-integral bridge are both established in the OpenSees environment and the seismic response analysis is carried out by the nonlinear time-history analysis. The parametric study of the APS is implemented and design guidance is suggested according to the results.

2. APPROACH PAVEMENT SYSTEM AND MODELING

The schematic diagram of the innovative fully jointless semi-integral bridge is shown in Figure 1. The continuous girder (deck), the approach slab, the reinforced concrete approach pavement and anchored ground beam are in series connection and the road surface layer which is usually made of asphalt concrete is completely smooth and jointless. The deformation or movement of the superstructure is freely transferred to the end of the approach slab which is integrated with the continous deck and cross over the top of the abutment back wall; the continous beam is not integrated with the abutment like the integral or semi-integral abutment briege, but is kept like the conventional beam bridge to avoid disturbing the backfill and pile foundation; the RCAP is set between the approach slab and anchored ground beam and the preseted cracks are evenly distributed in the RCAP which can accommodate the total deformation like a spring. The FJSIB should be completed at the high temperature season to ensure the RCAP in tension. Therefore the the thermal expansion/contraction of the FJSIB will not cause disruption to the soil around the anchor beams and approach pavements. The fully jointless semi-integral bridge is improved from conventional jointless bridge and to achive the goal of "the only good joint is no joint" (Kunin and Alampalli 2000). The fully jointless semi-integral bridge are better than the conventional jointless bridge in not only the driving quality, economy, durability and appearance but also the seismic performance and construction convenience. This excellent jointless bridge is used more and more in China and one real example which is builded in Kunming as shown in Figure 2.

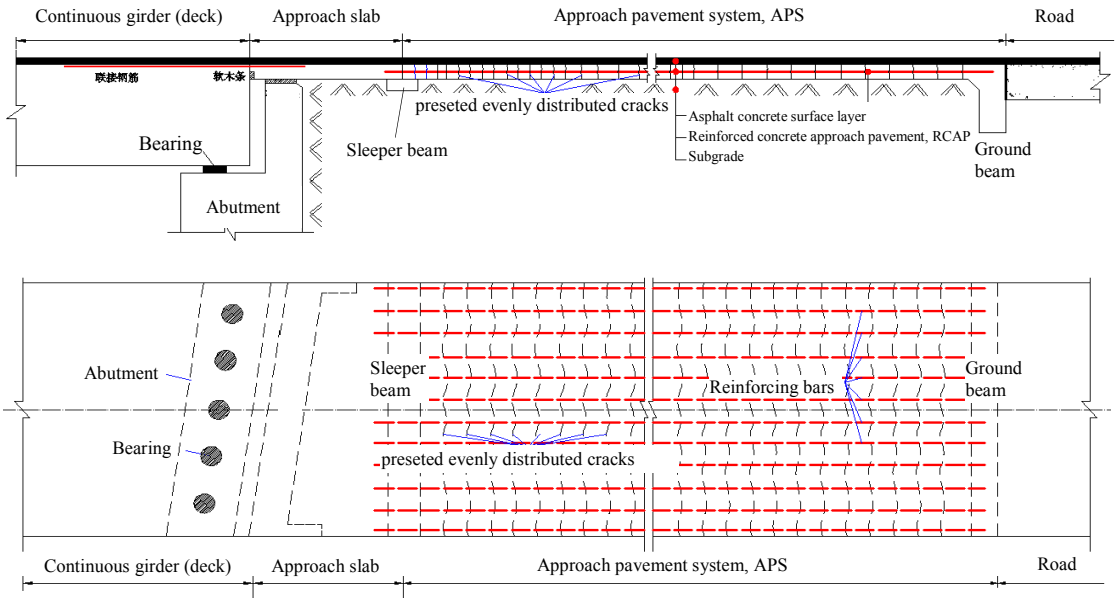

Figure 1. Fully jointless semi-integral bridge system: (a) elevation, (b) plan

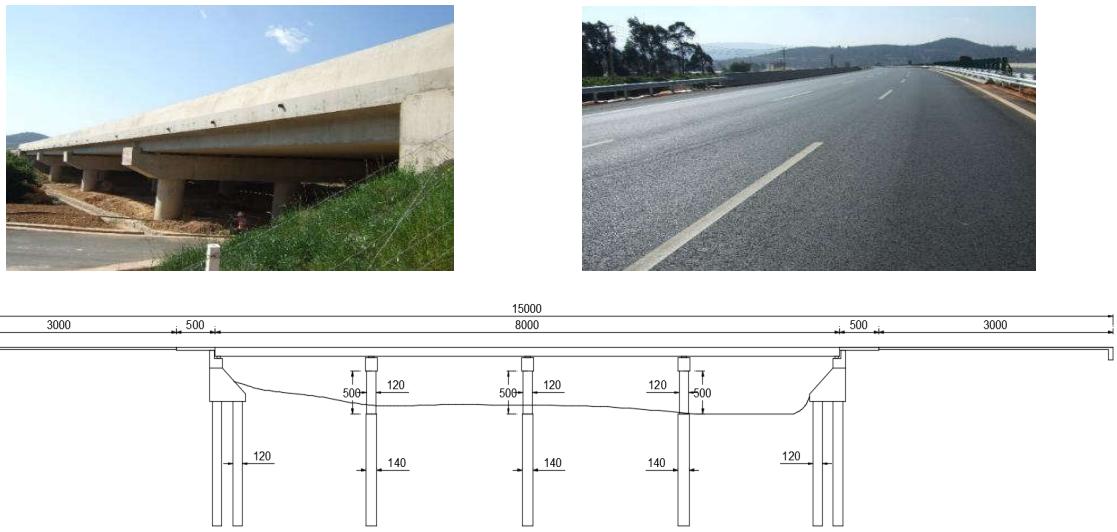

Figure 2. As-built fully jointless semi-integral bridge in Kunming: (a) elevation, (b) plan, (c)size (cm)

Obviously, the approach pavement system is the most distinctive component of the FJSIB and is crucial to the static and dynamic performance of the bridge. The approach pavement system consists of two element: (1) the reinforced concrete approach pavement and (2) the anchored ground beam. When the deck moves away from or is close to the abutment in the longitudinal direction due to the earthquake, the responses of APS include: (1) relative slip occurs between the RCAP and subgrade; (2) the reinforced concrete approach pavement is in the state of axial tension or compression; (3) the ground beam anchored by embankment is cyclically pulled and pushed by the RCAP. The nonlinear mechanics and modeling of the three parts will be described in details below.

2.1 Interfacial friction effect between RCAP and subgrade

The interfacial friction caused by the relative slip between RCAP and subgrade can consume the seismic energy and constrain the movement of the superstructure. Meanwhile, the interfacial friction also influences the internal force of the RCAP. The function of the subgrade to the RCAP (and the approach slab) includes two aspects: (1) vertical support; (2) horizontal friction. The “Flat Slider Bearing Element” of the OPENSEES can realize the two functions simultaneously (Mazzoni et al. 2006). The axial material of the element adopts the “Elastic-No Tension Material” to achieve the vertical support and the initial stiffness should be a maximum value. The shear material of the element adopts rigid plastic model to describe the Coulomb Friction effect and the coefficient of friction (μ) is 1.8 from tests (Jin and Shao 2009).

2.2 Reinforced concrete approach pavement

It is well known that the development of the stress, strain and crack of the reinforced concrete member after cracking, especially after the yielding of the reinforced bar, is very complicated. If the RCAP is simulated by the solid finite element or the nonlinear multi-layer shell in micro level, the accurate crack model, 3D/2D nonlinear material constitutive models of rebar and concrete and local bond-slip model, which are still not mature, must be given. Meanwhile, the nonlinear time history analysis of these microscopic models is time-consuming and there is a problem of convergence and stability. In this paper, to avoid these temporary insurmountable problems, discrete cracks of the RCAP are represented as "smeared" over a finite length rather than treated explicitly from the macro level; the constitutive behavior of the cross section is explicitly derived by discretization of the cross section into fibers; the plane sections remain plane, such that the strain distributes over the cross section linearly; the material constitutive models of the rebar fiber and concrete fiber adopt the simple uniaxial stress-strain model. A fiber force-based beam-column element for seismic response analysis of reinforced concrete structure which has been embedded into OpenSees coincides with this idea and can be used for efficient and robust calculation (Spacone et al. 1996[a], Spacone et al. 1996[b]).

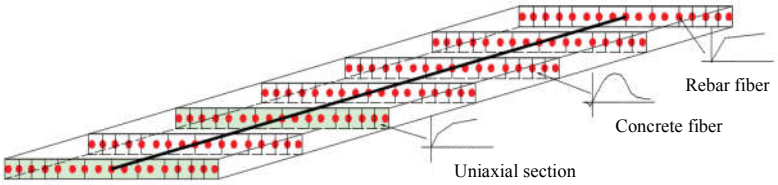

Figure 3. Element divison and section fiber division of the RCAP

In this paper, the RCAP is 30m long and divided into a number of elements which are modeled by the force-based beam-column element; the cross section is also discrete into multiple fibers, as shown in Figure 3. To predict the development of plasticity of RCAP, the Gauss-Lobatto integral method which is the most commonly used method for distributed plastic integral at present is adopted and each element selects 5 integration points. The accuracy of the seismic response analysis largely depends on the material constitutive models of the fibers. Based on a large number of experiments, Tamai 1988, Belarbi and Hsu 1994 proposed an average (smeared) uniaxial stress-strain model of the rebar and concrete which have been widely accepted, as shown in Figure 4. This steel and concrete constitutive models are modeled by the "SteelMPF" and "ConcreteCM" in OpenSees, respectively. The rebar and concrete of the RCAP are HRB335 and C30 respectively and the corresponding parameter values are shown in Table 1 and Table 2.

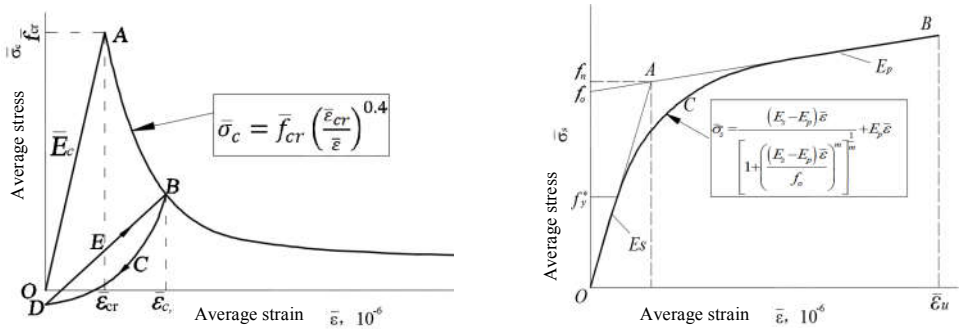

Figure 4. Average uniaxial tension stress-strain model: (a) concrete, (b) steel bar

Table 1. Parameter values of the SteelMPF for the RCAP

$E0 (MPa)	$fyn (MPa)	$fyp (MPa)	$bn	$bp
2.0×10^5	388	353	1%	2%

Table 2. Parameter values of the ConcreteCM for the RCAP

$Ec (MPa)	$fpcc (MPa)	$epcc ($10^{-6}$)	$rc	$ft (MPa)	$et ($10^{-6}$)	$rt
29722	31	2000	4.1	0.8	800	1.2

The internal force distribution of the RCAP under actual situation and the finite element model are shown in Figure 5 and it can be seen that the degree of element division has a great influence on the internal force of RCAP. Therefore a RCAP is modeled by element with length of 0.1m, 0.5m, 1.0m, 2.0m and 5.0m respectively and pushover analysis and nonlinear dynamic time-history analysis are carried out to determine the reasonable element length. The P-Δcurves of pushover analysis are shown in Figure 6. When the deformation (Δ) of the RCAP is small, the element length has little influence on the result, but when the large plastic deformation occurs, the curve of the element length of 5m is distinctly different from other element length. So for the static analysis of RCAP, element length$\leqslant$2m is sufficient to ensure the reliability of the modelling. The Δ-t curves of nonlinear dynamic time-history analysis are shown in Figure 7. It can be seen that: (1) the characteristic of the Δ-time curves

are similar but the discreteness of the response is much larger than in the pushover analysis; (2) when the element length⩽1m, peak response is basically stable and consistent. So for the dynamic analysis of RCAP, element length⩽1m is sufficient to ensure the reliability of the modelling.

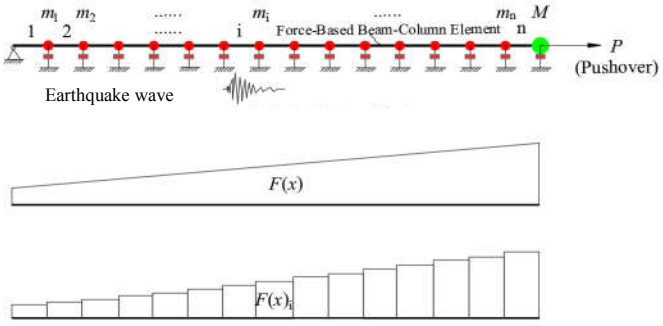

Figure 5. Internal force distribution of the RCAP: (a) element division, (b) actual, (c) FEM

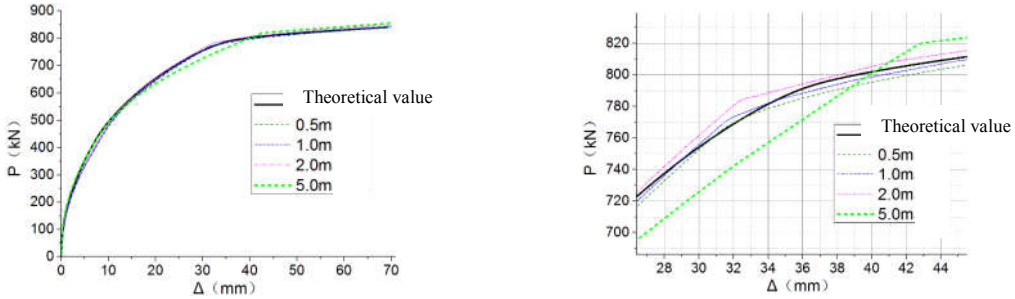

Figure 6. Pushover and analytical P-Δ curves of the RCAP: (a) full curve, (b) local curve

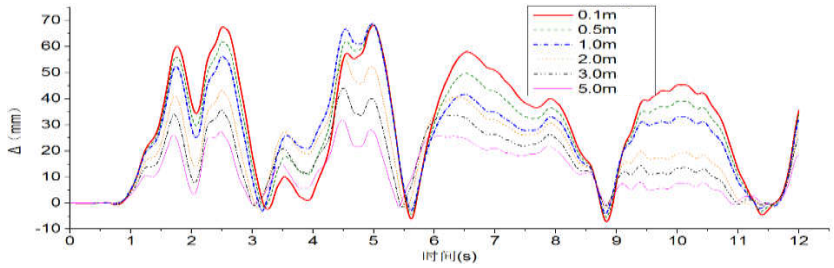

Figure 7. Δ-time curves of the RCAP under different element length

2.3 Soil-anchored ground beam interaction

The ground beam embedded in embankment is to anchor the end of RCAP and ensure the pavement jointless. The soil-anchored ground beam interaction belongs to the category of soil-rigid retaining wall interaction. So far, there are 6 main types of nonlinear soil spring model: Maragakis model (Maragakis 1984), NCHRP(1991) model (Barker et al. 1991), Caltrans model (Caltrans 2006), Log-spiral hyperbolic model, LSH (Shamsabadi et al. 2005), Hyperbolic force-displacement formulation, HFD (Shamsabadi et al. 2007), and Extended hyperbolic force-displacement formulation model, EHFD (Shamsabadi et al. 2010). The NCHRP and Maragakis models are used to establish the discrete distributional soil springs along the depth of the retaining wall. The NCHRP model is a form of curve + horizontal line, while the Maragakis model is a form of slash+horizontal line. The Caltrans model, the LSH model, the HFD model and the EHFD model are all used to establish the concentrated soil spring of the retaining wall. The Caltrans model is also an ideal elastoplastic model of the slash + horizontal straight line, which is simplified directly from the experimental results and does not involve any soil parameters; The LSH model, the HFD model and the EHFD model are a series of models, all of which are in hyperbolic form. The LSH model introduces the soil parameters and can calculate the

nonlinear model of various soils. In order to facilitate the engineering application, the HFD model and EHFD model adopt the simple functional descriptions of the LSH curve, and the EHFD model also introduces the height adjustment coefficient.

Based on the experiments of UCLA (Stewart et al. 2007, Lemnitzer et al. 2009) and UCD (Romstad et al. 1995), a retaining wall with a height equal to 1.67m and width equal to 1.00m is taken as the calculation model. The earth pressure-displacement curves obtained from the above 5 models (LSH model is not considered) are compared, as shown in Figure 8.

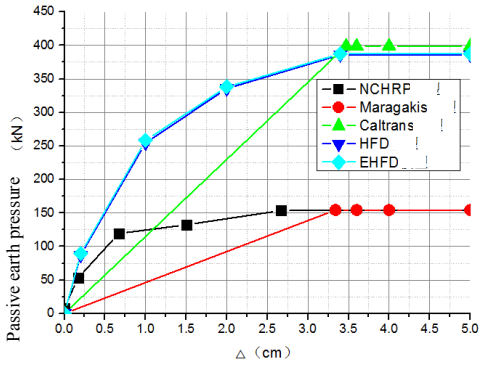

Figure 8. Nonlinear earth pressure- Δ curves of different models

It can be seen that NCHRP(1991) model and Maragakis model are conservative and the EHFD model is the rational model for modeling the soil-ground beam interaction. The expression of the EHFD is (Shamsabadi et al. 2010)

$$F(y)=\begin{cases}\dfrac{410.6y}{(H/1\mathrm{m})+1.867y}\left(\dfrac{H}{1\mathrm{m}}\right)^{1.56} & y\le 0.05H\ (\text{UCLA}\quad \text{Granular soil})\\ \dfrac{249.1y}{(H/1\mathrm{m})+0.8405y}\left(\dfrac{H}{1\mathrm{m}}\right)^{1.05} & y\le 0.10H\ (\text{UCD}\quad \text{Cohesive soil})\end{cases} \tag{1}$$

where, y is the horizontal displacement of the ground beam, cm; H is the height of the ground beam, m; F(y) is the earth pressure, kN. The anchored ground beam is modeled by elastic beam column element and ZeroLength Element with HyperbolicGapMaterial developed from EHFD model is used to model the soil-ground beam interaction. The HyperbolicGapMaterial is shown in Figure 9 and the parameter values in this paper are: H =1.5m and $Kur=$Kmax=45823kN/m, $Rf=0.7, $Fult=374kN (per metre width).

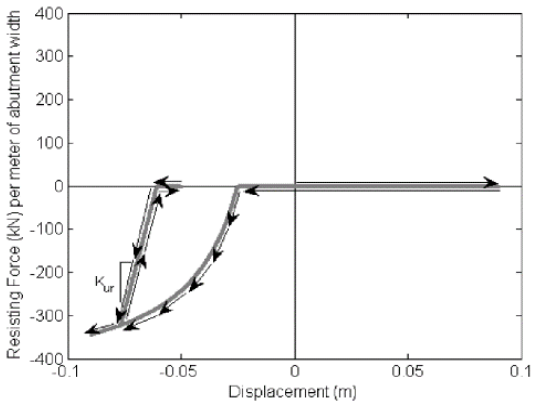

Figure 9. HyperbolicGapMaterial

3. ANALYTICAL MODELING OF THE ANALYZED BRIDGE SYSTEMS

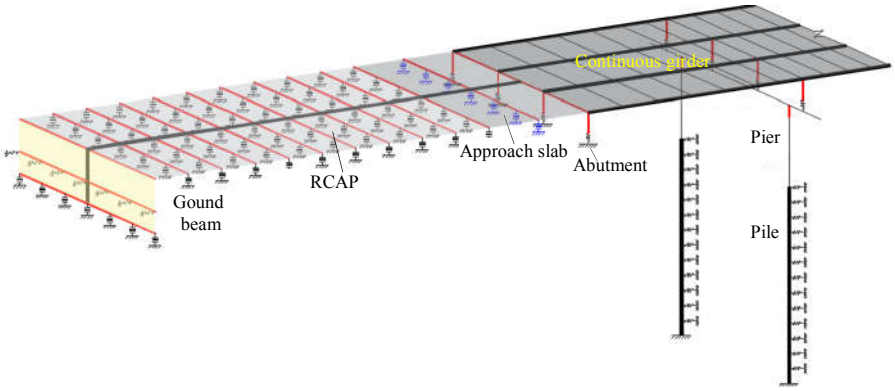

Figure 10. Stick nonlinear finite element model of the FJSIB

The "reference" bridge is a 4×20m continuous girder bridge (CGB) and the corresponding FJSIB is shown in Figure 2. The simplified nonlinear finite element model of CGB and FJSIB are both created in OpenSees. The girders, bent caps and piles of the bridge are modeled by elastic beam column element. The "red lines" in Figure 10 represent the rigidlink element. An experiment has proven that the approach slabs is elastic when the RCAP is tensile failure (Ma et al. 2012). Therefore the approach slabs can be modeled by elastic timoshenko beam column element. The elastomeric bearings are modeled by elastomericBearingPlasticity of OpenSees. The piers are modeled by force-based beam-column element with the modified radau hinge integration which not only can overcome strain softening but also can consider the plastic distribution (Scott and Fenves 2006). The plastic hinge length L_p can be calculated according to (Paulay and Priestley 1992):

$$L_p = \min\begin{cases} 0.08L + 0.022 f_y d_b \geq 0.044 f_y d_b \\ \dfrac{2}{3} b \end{cases} \quad \text{(N, mm)} \tag{2}$$

where, L is the length of pier; f_y, d_b is the yield strength and diameter of the longitudinal reinforcing steel bar respectively; b is the width of the short side of a rectangular section or the diameter of a circular section. In this paper, the L=5000mm, d_b=25mm, f_y=388N/mm2, b =1200mm and L_p =673mm. The fibers of steel bar and concrete of the piers are modeled by SteelMPF and ConcreteCM of the OpenSees. The ConcreteCM is developed according to the Mander model (Mander et al. 1988) which can consider the confined concrete of the piers. The parameter values of the SteelMPF and ConcreteCM are shown in Table 3 and Table 4. The soil-pile interaction is model by the zero-Length element with PySimple1 based on Boulanger nonlinear dynamic p-y model (Boulanger et al. 1999). The stick nonlinear finite element model of FJSIB is shown in Figure 10. The difference between continuous girder bridge and fully jointless semi-integral bridge is the approach pavement system.

Table 3. Parameter values of the SteelMPF for the pier

$E0 (MPa)	$fyn (MPa)	$fyp (MPa)	$bn	$bp
2.0×10^5	388	388	1%	1%

Table 4. Parameter values of the ConcreteCM for the pier

	$Ec (MPa)	$fpcc (MPa)	$epcc ($10^{-6}$)	$rc	$ft (MPa)	$et ($10^{-6}$)	$rt
I	29722	31	2000	4.1	0	0	0
II	27838	34	2393	4.3	3.4	124	1.3

Notes: I is the non constrained concrete for protective layer, II is the constrain concrete for the core area of pier column.

4. EARTHQUAKE MOTION

Ten earthquake waves, shown in Table 5, are selected from strong earthquake record database of PEER and CSMNC according to site condition, fault distance and effective period etc. The peak ground acceleration is set to 0.07g, 0.13g and 0.26g corresponding to the minor, medium and major earthquakes, respectively. Dynamic non-linear time history analysis is implemented and the direct integration, known as β-Newmark method, is used as this method is the most robust for the step-by-step dynamic analysis.

Table 5. Properties of the selected earthquake waves

No.	Magnitude	year	name	V_s_30 (m/s)	distance (km)	PGA (g)	PGV (cm/s)	T_d (s)
1	6.50	1976	Friuli, Italy-01	424.8	14.97	0.31	30.78	4.9
2	6.53	1979	Imperial alley-06	274.5	22.03	0.35	32.99	50.3
3	6.54	1987	Superst Hills- 02	207.5	23.85	0.21	34.51	28.7
4	6.93	1989	Loma Prieta	370.8	27.67	0.37	62.30	16.4
5	7.28	1992	Landers	353.6	23.62	0.24	51.40	17.6
6	6.69	1994	Northridge-01	450.3	20.10	0.57	52.54	9.1
7	6.90	1995	Kobe,Japan	256.0	19.14	0.24	37.84	10.3
8	7.14	1999	Duzce,Turkey	326.0	12.02	0.82	62.07	9.4
9	7.62	1999	Chi-Chi	446.6	45.15	0.38	62.02	13.2
10	8.00	2008	Wenchun,China	300.0	18.76	0.48	35.87	72.0

Notes：Vs_30 is the mean shear wave velocity for 30m soil layer。

5. ANALYTICAL RESULTS AND DISCUSSION

The maximum value of the seismic response is considered for the continuous girder bridge and the fully jointless semi-integral bridge. The analytical results are the average value of the 10 maximum values corresponding to the 10 earthquake waves. A total of 30 (=3×10) analysis cases are performed for the two bridge systems. To coincide with the displacement-based seismic design (DBSD), the seismic responses are represented as the displacement or in deformation in Table 6. To assess the damage state, different damage levels for ground beam, RCAP, bearing and pier are calculated in Table 7.

Under the minor earthquake (0.07g), Table 6 and Table 7 show that: (i) the movement of the ground beam is 0 and the tensile deformation of RCAP is 6.1mm≈12/2mm. It indicates that the seismic response of the approach pavement system is within the serviceability limit state under minor earthquake. (ii) the deformations of bearing, pier of the two bridges are all in elastic state. The seismic response of FJSIB is reduced significantly, compared to continuous girder bridge, especially in longitudinal direction.

Under the medium earthquake (0.13g), Table 6 and Table 7 show that: (i) the movement of the ground beam is 0.5mm<1.0mm and the tensile deformation of RCAP is 9.7mm>12/2mm. It indicates that the ground beam is disturbed by the RCAP where the asphalt pavement is still not cracking under medium earthquake; however, the slight tension damage of the RCAP appears, which may lead to develop microcrack in asphalt pavement. (ii) the deformations of bearing, pier of the two bridges are still in elastic state. The deformation of the bearing of the continuous girder bridge is 41.9mm which is close to 45mm and is goes beyond the elastic limit while the deformation of the bearing of the FJSIB is only 13% of the CGB.

Under the major earthquake (0.26g), Table 6 and Table 7 show that: (i) the movement of the ground

beam is 8.4mm>5.0mm and the tensile deformation of RCAP is 16.6mm and 12/2mm<16.6mm <35-12/2=29mm. It indicates that large plastic deformation of embankment is introduced under the major earthquake where the asphalt pavement cracks completely. However, the steel bar of the RCAP is still in the elastic phase and the cracks can be closed by themselves after unloading. (ii) The deformation of the bearing of the continuous girder bridge is 96.1mm>90mm and the bearing is damaged severely while the bearing of the FJSIB deforms only 10mm<45mm and is still excellent without damage.

It can be obtained that the seismic response of the fully jointless semi-integral bridge is significantly reduced by the approach pavement system under the three earthquake levels, especially in the longitudinal direction. Under the major earthquake, the fully jointless semi-integral bridge is in excellent condition except the asphalt pavement at the ground beam is damaged. Meanwhile the abutment and the expansion joints of the continuous girder bridge is punching shear failure by the strong inertia force from the girder; the bearings are also damaged severely and even induce falling beam destruction; the plastic hinges are also developed in the piers.

Table 6. Seismic response of FJSIB and CGB at three earthquake levels （mm）

Component	Minor earthquake			Medium earthquake			Major earthquake		
	FJSIB	CGB	$\frac{\text{FJSIB}}{\text{CGB}}$	FJSIB	CGB	$\frac{\text{FJSIB}}{\text{CGB}}$	FJSIB	CGB	$\frac{\text{FJSIB}}{\text{CGB}}$
Ground beam	0.0	—	—	0.5	—	—	8.4	—	—
RCAP	6.1	—	—	9.7	—	—	16.6	—	—
Bearing-on pier	3.7	21.2	17%	5.4	41.9	13%	10.0	96.1	10%
Pier- longitudinal	2.6	5.7	47%	5.0	9.2	55%	9.0	14.7	61%
Pier-transverse	2.6	3.2	81%	5.0	6.9	72%	11.5	13.3	86%

Table 7. Different damage level for each component （mm）

Component	Slight damage	Medium damage	Severe damage	Complete damage
Pier- longitudinal	23	30	65	134
Pier-transverse	11	15	48	82
Bearing-on pier	45	68	90	113
Ground beam	1	5	30	
RCAP	12	35	69	106

Table 8. Seismic responses of the FJSIB with different ground beam

Conponent	PGA=0.26g			PGA=0.39g			PGA=0.52g		
	A	B	B/A	A	B	B/A	A	B	B/A
Ground beam(mm)	8.4	6.0	0.7	16.9	13.0	0.8	26.3	21.1	0.8
Bearing-abutment(mm)	13.5	12.1	0.9	22.8	19.4	0.9	32.7	28.5	0.9
Bearing-pier(mm)	10.0	10.4	1.0	18.1	15.2	0.8	26.0	23.5	0.9
pier(mm)	9.0	9.5	1.1	13.2	13.7	1.0	17.6	18.1	1.0
RCAP(mm)	16.6	16.6	1.0	22.7	22.3	1.0	28.2	28.9	1.0
Girder-moment(kN·m)	424.3	530.6	1.3	500.1	655.4	1.3	606.1	778.9	1.3

Notes: A represents the one ground beam; B represents the two ground beam.

6. PARAMETRIC STUDY

Obviously, the stiffness of the anchored ground beam is the sensitive parameter for seismic response and it is necessary to determine the optimal stiffness of the soil-ground beam interaction. Therefore a

parametric investigation is conducted and 1 and 2 ground beams are set to consider different stiffness of the soil- ground beam interaction, and the FJSIB is under 0.26g, 0.39g and 0.52g earthquake action. The calculated results are shown in Table 8. It can be seen that 2 ground beams can slightly reduce the seismic response of the ground beam and bearing and can also slightly increase the moment of the girder, while the deformation of the RCAP is almost not changed. It is suggested that one ground beam is enough and more ground beams will not lead to the better result.

7. CONCLUSION

The 3D nonlinear finite element model of FJSIB and CGB are established by the OpenSees software and the seismic response analysis is carried out by the nonlinear time-history analysis. It is proved that the approach pavement system can significantly enhance the earthquake resistance of the minor and medium beam bridges. Under the major earthquake, except the asphalt pavement at the ground beam is damaged which is easy to repair, the fully jointless semi-integral bridge is in excellent condition. While the abutment wall, expansion joints, bearings and piers of the "reference" continuous girder bridge are damaged severely in major earthquake. From the parametric study, it is found that one ground beam is enough and more ground beams will not lead to the better performance. It can be concluded that the fully jointless semi-integral bridge have excellent seismic performance and can be used in new bridge construction as well as old bridge retrofitting, especially in the strong earthquake area.

8. ACKNOWLEDGEMENT

The authors gratefully acknowledge the support from the National Natural Science Foundation of China (Grant No. 51608190 and 51708205) and Natural Science Foundation of Hunan Province of China (Grant No. 2017JJ3058).

9. REFERENCES

Boulanger R W, Curras C J, Kutter B L, et al (1999). Seismic soil-pile-structure interaction experiments and analyses. *Journal of Geotechnical and Geoenvironmental Engineering*, 125(9): 750-759.

Belarbi A, Hsu T T (1994). Constitutive laws of concrete in tension and reinforcing bars stiffened by concrete. *ACI structural Journal*, 91(4): 465-474.

Barker R, Duncan J, Rojiani K, et al (1991). National Cooperative Highway Research Program(NCHRP) Report 343: Manuals for the design of bridge foundations. Washington D.C.: *Transportation Research Board*.

Maruri R F, Petro S H (2005). Integral abutments and jointless bridges (IAJB) 2004 survey summary. In: *Integral Abutment and Jointless Bridges (IAJB 2005*).

Ma Y, Shao X, Yu J (2013). seismic analysis of the fully jointless bridge in the low seismic fortification intensity zone. *Journal of Hunan University (Natural Sciences)*, 40(5): 11-17.

Ma Y, Shao X, Liang C (2012). Theoretical and experimental study on tension-deformation mechanical properties of continuously reinforced concrete approach pavement of FJSBs. *Journal of Earthquake Engineering and Engineering Vibration*, 32(04): 131-138.

Jin X, Shao X (2009). A study of fully jointless bridge-approach system with semi-integral abutment. *China Civil Engineering Journal*, 42(09): 68-73.

Hoppe E J, Gomez J P (1996). Field study of an integral backwall bridge. Virginia: *Transportation Research Council*, pp 47.

Faraji S, Ting J M, Crovo D S, et al (2001). Nonlinear analysis of integral bridges: finite-element model. *Journal of Geotechnical and Geoenvironmental Engineering*, 127(5): 454-461.

Ní Choine M, O'Connor A J, Padgett J E (2015). Comparison between the Seismic Performance of Integral and Jointed Concrete Bridges. *Journal of Earthquake Engineering*, 19(1): 172-191.

Kunin J, Alampalli S (2000). Integral abutment bridges: Current practice in United States and Canada. *Journal of performance of constructed facilities*, 14(3): 104-111.

Mazzoni S, McKenna F, Scott M H, et al (2006). OpenSees: Open system for earthquake engineering simulation. Pacific Earthquake Engineering Research Center, California, Berkeley.

Spacone E, Filippou F C, Taucer F F (1996[a]). Fibre beam-column model for non-linear analysis of R/C frames: Part I. Formulation. *Earthquake Engineering and Structural Dynamics*, 25(7): 711-726.

Spacone E, Filippou F C, Taucer F F (1996[b]). Fibre beam-column model for non-linear analysis of R/C frames: Part II. Applications. *Earthquake Engineering and Structural Dynamics*, 25(7): 727-742.

Tamai S, Shima H, Izumo J, et al (1988). Average stress-strain relationship in post yield range of steel bar in concrete. *Concrete Library of JSCE*, 11(June): 117-129.

Maragakis E (1984). A model for the rigid body motions of skew bridges. *Report No. EERL 85-02, Earthquake Engineering Research Laboratory*, Caltech, Pasadena.

Caltrans S (2006). Caltrans Seismic Design Criteria. California Department of Transportation, Sacramento, CA.

Shamsabadi A, Ashour M, Norris G (2005). Bridge abutment nonlinear force-displacement-capacity prediction for seismic design. *Journal of geotechnical and geoenvironmental engineering*, 131(2): 151-161.

Shamsabadi A, Rollins K M, Kapuskar M (2007). Nonlinear soil–abutment–bridge structure interaction for seismic performance-based design. *Journal of geotechnical and geoenvironmental engineering*, 133(6): 707-720.

Shamsabadi A, Khalili-Tehrani P, Stewart J P, et al (2010). Validated simulation models for lateral response of bridge abutments with typical backfills. *Journal of Bridge Engineering*, 15(3): 302-311.

Stewart J P, Taciroglu E, Wallace J W, et al (2007). Full scale cyclic testing of foundation support systems for highway bridges. Part II: Abutment backwalls. *Rep. No. UCLA-SGEL-2007/02*, *Structural and Geotechnical Engineering Laboratory*, Univ. of Calif., Los Angeles.

Lemnitzer A, Ahlberg E R, Nigbor R L, et al (2009). Lateral performance of full-scale bridge abutment wall with granular backfill. *Journal of geotechnical and geoenvironmental engineering,* 135(4): 506–514.

Romstad K, Kutter B, Maroney B, et al (1995). Experimental measurements of bridge abutment behavior. *Rep. No. UCD-STR-95-1*, Dept. of Civil and Environmental Eng., Univ. of California, Davis, Calif.

Scott M H, Fenves G L (2006). Plastic hinge integration methods for force-based beam–column elements. *Journal of Structural Engineering*, 132(2): 244-252.

Paulay T, Priestley M J N (1992). Seismic design of reinforced concrete and masonry buildings. New York: Wiley.

Mander J, Priestley M, Park R (1988). Observed Stress-Strain Behavior of Confined Concrete. *Journal of Structural Engineering*, 114(8): 1827-1849.

Wilson J C (1988). Stiffness of non-skew monolithic bridge abutments for seismic analysis. *Earthquake engineering & structural dynamics*, 16(6): 867-883.